# Chapter 4

# ~~Eighteen~~ Phases of Ice and Counting

*Alfred Amon, Bharvi Chikani, Siriney O. Halukeerthi, Carissa Ponan, Alexander Rosu-Finsen, Zainab Sharif, Rachael L. Smith, Sukhpreet K. Talewar* and *Christoph G. Salzmann**

## Introduction

$H_2O$ is the thermodynamically ~~most~~ stable combination of hydrogen and oxygen, and exists in vast quantities in our ~~u~~niverse (Tielens 2013). From the oceans on Earth and the poles of Mars to the icy moons of the gas giants and the distant mountain ranges of Pluto, $H_2O$ is a constant companion throughout our solar system and a critical ingredient for the evolution and support of life (Ball 1999). Although often depicted as a V-shaped molecule, the van der Waals volume of the water molecule is dominated by the oxygen atom with two 'bulges' where the two hydrogen atoms are located (Finney 2001). Unlike any of the other dihydrogen chalcogenides, $H_2O$ is capable of forming up to four hydrogen bonds with neighboring molecules which has a pronounced impact on the physical properties of its condensed phases including the temperatures of melting and boiling (Petrenko and Whitworth 1999).

The familiar hexagonal phase of ice is called ice I*h*. Based on X-ray diffraction, it was established that the oxygen atoms in ice I*h* are arranged in tetrahedral coordination environments (Dennison 1921, Bragg 1921, Barnes and Bragg 1929). However, the positions of the hydrogen atoms remained unresolved and even controversial until the late 1940s when neutron diffraction became available (Wollan et al. 1949). Four of the debated structural models are shown in Fig. 1. According to the Barnes model (Barnes and Bragg 1929), the water molecules lose their molecular character in ice with hydrogen atoms located halfway between the oxygen atoms. The Bernal-Fowler model on the other hand suggested intact and orientationally ordered $H_2O$ molecules (Bernal and Fowler 1933). Pauling proposed a structural

Department of Chemistry, University College London, 20 Gordon Street, London WC1H 0AJ, UK.
* Corresponding author: c.salzmann@ucl.ac.uk

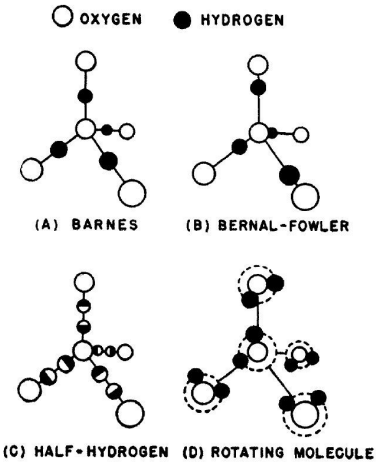


**Fig. 1:** The four ~~possible~~ structural models used to analyze the first powder neutron diffraction data of $D_2O$ ice I*h* (Barnes and Bragg 1929, Bernal and Fowler 1933, Pauling 1935, Wollan et al. 1949). Reproduced with permission from Wollan et al. (1949).

model with two half-occupied hydrogen sites along each of the hydrogen bonds (Pauling 1935). Finally, rotating water molecules, in what would now be considered a plastic phase of ice, were considered as well (Wollan et al. 1949). The analysis of the powder neutron diffraction of data of $D_2O$ ice I*h* revealed that Pauling's model provides the best match to the recorded intensities of the Bragg peaks. The half-occupied hydrogen sites thereby reflect the average structure of ice in which the orientations of the fully hydrogen-bonded water molecules are random. Such an ice structure is commonly described as hydrogen disordered. The molar configurational entropy of such a phase of ice was estimated by Pauling as $R$ ln (3/2) (Pauling 1935). The frequently used term "proton disordered" is chemically incorrect since the water molecule contains hydrogen atoms and not ~~protons, that is,~~ $H^+$ ions.

In addition to ice I*h*, several other phases of ice exist that have been labelled with increasing Roman numerals in chronological order of their discoveries. The up-to-date phase diagram of ice is shown in Fig. 2. Like ice I*h*, all other phases of ice that share phase boundaries with liquid water including ices III, V, VI, and VII are hydrogen disordered and hence follow Pauling's model. Despite not being able to reproduce the diffraction pattern of ice I*h*, the other three structural models shown in Fig. 1 still turned out to be highly relevant for ice research. Upon cooling, the hydrogen-disordered ices III and VII transform to their hydrogen-ordered counterparts, ices IX and VIII with defined orientations in line with the Bernal-Fowler model (La Placa and Hamilton 1973, Whalley et al. 1968, Whalley et al. 1966). Compression of ice VII beyond 60 GPa leads to the formation of ice X as the hydrogen bonds become symmetric like in the Barnes model (Stillinger and Schweitzer 1983, Polian and Grimsditch 1984). The formation of a plastic state of ice VII at high temperatures has been suggested (Takii et al. 2008, Aragones and Vega 2009, Hernandez and Caracas 2018) and the recently discovered superionic ice XVIII (Millot et al. 2018, Millot et al. 2019) can even be seen as a state beyond plastic rotations with completely dissociated water molecules.

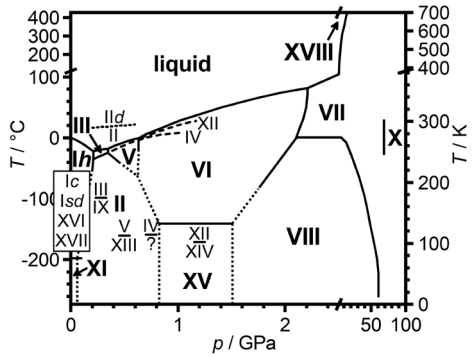


**Fig. 2:** The phase diagram of ice. Phases in their regions of stability are shown as bold Roman numerals whereas a smaller font size is used for metastable phases. Dashed lines indicate metastable melting lines whereas dotted lines are either extrapolated or estimated computationally (Nakamura et al. 2016).

The hydrogen-bonded networks of all phases of ice discovered so far are shown in Fig. 3. A complex array of structures exists, ranging from ices I*h*/XI, II, and XVII with large open channels to the densely knit interpenetrating networks of ices VI/XV

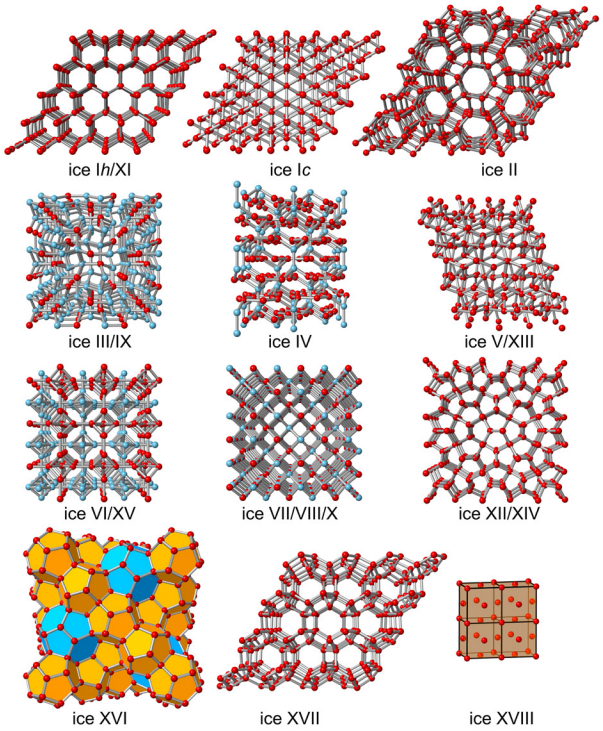


**Fig. 3:** The hydrogen-bonded networks of the various phases of ice. Oxygen atoms are shown as spheres and hydrogen bonds as grey lines. Blue spheres indicate the oxygen atoms belonging to 4-fold spirals in ice III/IX, interpenetrating hydrogen bonds in ice IV, and the second independent networks in ices VI/XV and VII/VIII/X. The structure of ice I*c* is shown with the corresponding supercell of ice I*h*. The orange and blue polyhedra in ice XVI indicate the two different types of cages. The unit cell of the superionic ice XVIII is shown with black lines.

and VII/VIII/X (Salzmann 2019). In the following sections, the various phases of ice will be introduced by describing their structures, physical properties, and the most recent experimental advances in understanding these phases.

## The Ice I Family of Polytypes

Hexagonal ice I*h* is the most ubiquitous, naturally occurring form of ice on Earth which forms below 0ºC at atmospheric pressure (Kuhs and Lehmann 1983, Röttger et al. 1994). The crystal structure of ice I*h* with space group $P6_3/mmc$ contains puckered layers of six-membered rings of water molecules in the chair conformation as shown in Fig. 4(a). These layers extend in the *a*-*b*-plane and are stacked along the *c*-axis where each layer is the mirror image of the previous layer. The hexagonal stacking of layers is indicated by 'h' in Fig. 4(b). Due to the stacking, six-membered rings in the boat conformation are formed so that the ice I*h* structure contains equal amounts of six-membered rings in the chair and boat conformations. The hexagonal unit cell of ice I*h* contains 4 water molecules and one distinct oxygen site. Although of very similar length, two different types of hydrogen bonds exist in ice I*h*: those within the layers and those connecting them. Ice I*h* is fully hydrogen disordered and it has been discussed that the hydrogen disorder induces positional disorder of the oxygen atoms (Bertie and Whalley 1964a, Kuhs and Lehmann 1983). Highly accurate measurements of the lattice constants of ice I*h* as a function of temperature have recently been reported (Fortes 2018). Furthermore, insights into the reorientation dynamics and weak ordering processes at low temperatures have been gained from measurement of the lattice constants (Fortes 2019). Below ~ 60 K, ice I*h* displays negative thermal expansion (Röttger et al. 1994, Gupta et al. 2018).

The crystal structure of ice I*c* with space group *Fd*-3*m* comprises layers identical to those in ice I*h* but they are stacked on top of one another by shifting halfway across

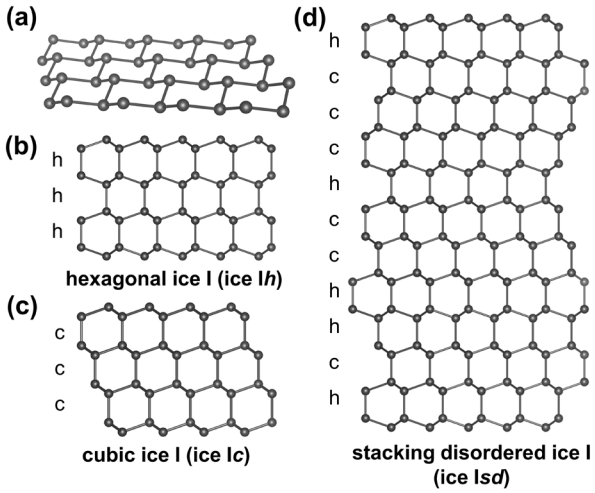


**Fig. 4:** Stacking of layers in ice I. (a) Single puckered ice I layer. Side views of the stacking of layers in (b) ice I*h*, (c) ice I*c*, and (d) stacking disordered ice I (ice I*sd*). Oxygen atoms of water molecules are shown as spheres, connected by hydrogen bonds drawn as lines. Hexagonal and cubic stacking is indicated as 'h' and 'c', respectively.

the diagonal of the six-membered rings (Kuhs et al. 1987). Cubic stacking is indicated by '*c*' in Fig. 4(c). The arrangement of oxygen atoms in ice I*c* is identical to the cubic diamond structure. Hence, the overall structure contains only six-membered rings in the armchair conformation. The cubic unit cell contains eight water molecules with one distinct oxygen site and one type of hydrogen bond. Since the structural difference between ice I*h* and I*c* lies only in the way that identical layers are stacked, these two forms of ice are not considered to be distinct polymorphs but different polytypes of ice I.

Pure cubic ice I*c* has been prepared for the first time in two recent independent studies. The first route involves heating the low-density ice XVII under vacuum to ~ 160 K (del Rosso et al. 2020). Alternatively, ice I*c* can be prepared by decompressing the $C_2$ high-pressure hydrogen hydrate to ambient pressure at ~ 100 K (Komatsu et al. 2020b). The host framework of the $C_2$ hydrate is isostructural with ice I*c* which may provide a templating effect for its formation. The recent discoveries of ice I*c* have now paved the way for detailed investigations of its physical properties and how they differ from those of ice I*h*. A rare 28º halo from the sun, called Scheiner's halo, has been suggested to arise from the presence of octahedral ice I*c* crystal in the atmosphere (Whalley 1983).

Before the recent discovery of ice I*c*, diffraction data of so-called 'cubic ice' samples always showed the evidence of mixing of cubic and hexagonal stacking in the form of diffuse diffraction features (Kuhs et al. 1987, Hansen et al. 2008, Malkin et al. 2012, Kuhs et al. 2012, Malkin et al. 2015, Amaya et al. 2017). The name 'stacking disordered' ice (ice I*sd*) was therefore suggested for this type of ice I, which allows varying fractions of cubic and hexagonal stacking ranging between pure ice I*h* and pure ice I*c* (Malkin et al. 2012). A possible stacking sequence of ice I*sd* is shown in Fig. 4d. The space group of ice I*sd* is *P*3*m*1 which could explain the rare occurrence of snowflakes with 3-fold rotational symmetry (Murray et al. 2015). Computational fitting of the diffraction data of ice I*sd* enables the determination of its cubicity (that is, the percentage of cubic stacking). Furthermore, information on memory effects in the stacking sequences can be obtained which is most usefully visualized with the help of the 'stackogram' plot (Hansen et al. 2008, Malkin et al. 2015, Salzmann et al. 2015). Independent of their cubicities, all ice I*sd* samples so far displayed a greater tendency to stay with a given type of stacking rather than switching. In addition to diffraction, stacking disorder in ice I can also be identified from the Raman spectrum (Carr et al. 2014).

Following the preparation of ice I*sd* using cryogenic vapor deposition (König 1943), subsequent routes included the recrystallisation of high-pressure phases, heating of low-density amorphous ice, and freezing of water and aqueous solutions (Mayer and Hallbrucker 1987, Kuhs et al. 2012, Malkin et al. 2015). The enthalpies of transformation to ice I*h* range from 23 to 160 J $mol^{-1}$ (Malkin et al. 2015, Handa et al. 1986). It seems possible that changes in the interfacial energies may contribute to the measured enthalpies (Handa et al. 1988).

Ice XI is the hydrogen-ordered counterpart of ice I*h* and forms below 72 K with the help of a base dopant (Tajima et al. 1982). Out of all alkali hydroxides, KOH was found to be the most effective dopant (Tajima et al. 1984, Matsuo and Suga 1987). The space group of ice XI is $Cmc2_1$, which makes it the only ferroelectric

phase of ice with a net dipole moment (Leadbetter et al. 1985, Howe and Whitworth 1989, Line and Whitworth 1996, Jackson et al. 1997). Its unit cell contains eight water molecules with two different oxygen sites and three types of hydrogen bonds. Complete hydrogen ordering of ice XI has so far not been achieved. For example, annealing a KOD-doped $D_2O$ ice I*h* sample at 70 K for 135 hours leads to a 58% weight fraction of ice XI (Fukazawa et al. 2005). The ice I*h* to XI phase transition has been shown to exhibit memory effects which means that once ice XI has been formed, it is easier to form it again from ice I*h* (Arakawa et al. 2011). The problems ~~of~~ achieving full hydrogen order in ice XI have been attributed to the strain ~~on~~ the ice I*h*/XI interface (Johari 1998). Acid dopants have been shown to be ineffective for preparing ice XI (Ueda et al. 1982, Matsuo and Suga 1987).

The possible existence of ice XI in space has been discussed (Fukazawa et al. 2006) and the ferroelectric nature of the ground state structure of ice I*h* has recently been challenged (Parkkinen et al. 2014). Furthermore, now that ice I*c* has been made, future work can focus on isolating its hydrogen-ordered counterpart for which several different structures have been discussed (Raza et al. 2011). In fact, hydrogen-ordered ice I*c* could potentially be the most polar state of condensed $H_2O$ with all dipole moments perfectly aligned.

In addition to ice I structures with extended hexagonal and cubic stacking, high-order polytypes are possible as well in principle. According to the Ramsdell notation, the 4H, 6H, and 9R polytype include periodic sequences of (hc), (hcc), and (hhc) blocks. If and how such polytypes of ice I can be prepared is ~~entirely~~ unclear at present. However, it may well be that the ice I family of polytypes will continue to grow in the future (Salzmann 2019).

## ~~I CeII~~: The Odd One Out?

Ice II was the first of the high-pressure phases of ice to be discovered (Tammann 1900, Bridgman 1912). Its rhombohedral unit cell with *R*-3 space group symmetry (Kamb 1964, Finch et al. 1968, Kamb et al. 1971) contains open channels akin to nanotubes that are hydrogen-bonded to one another (*cf.* Fig. 3) (Salzmann et al. 2011). The rhombohedral unit cell contains 12 water molecules, two distinct oxygen sites and four types of hydrogen bonds. The corresponding hexagonal cell has three times the volume and hence contains 36 molecules. The channels consist of two types of six-membered rings, one significantly puckered and the other one almost flat, that are stacked in an alternating fashion. Eight and ten-membered rings exist between adjacent channels. Upon compression, ice II displays anisotropic changes in its structure (Fortes et al. 2003).

The open channels of ice II can be filled with hydrogen (Dyadin et al. 1999), helium (Londono et al. 1992, Lobban et al. 2002), and neon (Yu et al. 2014) which stabilizes the ice II structure with respect to ices III and V. In contrast to its neighboring phases in the phase diagram, ice II is fully hydrogen ordered (Kamb et al. 1971, La Placa and Hamilton 1973, Arnold et al. 1971, Lobban et al. 2002). This is remarkable considering that its triple point with ices III and V is only ~ 5 K away from the melting line (Journaux et al. 2020). The complete hydrogen order of ice II was also confirmed spectroscopically (Bertie and Whalley 1964b, Bertie et al.

1968a, Bertie and Francis 1980, 1982, Minceva-Sukarova et al. 1985, Li et al. 1991, Tran et al. 2017). Its compressibility and thermal expansion under *in situ* conditions has been studied using neutron diffraction (Fortes et al. 2005).

The thermal stability of the hydrogen-ordered ice II means that it is the only phase of ice for which the hydrogen-disordered counterpart is unknown. Upon heating ice II, it transforms to ices I, III, V, or VI depending on the pressure and not to its hydrogen-disordered counterpart (*cf*. Fig. 2). It has been ~~shown~~ computationally that the phase transition from ice II to its disordered counterpart ice II*d* takes place at *p*/*T* conditions where liquid water is the stable phase (Nakamura et al. 2016). The space group of ice II*d* has been suggested as *R*-3c (Kamb 1973) although it should be noted that ice II can also appear to have this space group because of twinning (Kamb 1964). In addition to a perfectly hydrogen-ordered structure, dielectric spectroscopy suggests a complete lack of defects and a static structure in stark contrast to the hydrogen-disordered ices (Wilson et al. 1965). The lack of defects could also explain why ice II is much harder compared to its neighbors in the phase diagram which could have an impact on the geophysics of icy moons (Echelmeyer and Kamb 1986, Durham et al. 1997). Upon heating at ambient pressure, ice II is the only phase of ice displaying an endothermic phase transition to ice I*sd*, again illustrating its stability (Handa et al. 1988). Out of all the high-pressure phases, it also gives the ice I*sd* with the highest cubicity (Malkin et al. 2015). Whalley et al. (1965) stated that "the complexity of the phase diagram of ice is due largely to ice II being ordered at all temperatures".

Recently it was discovered that doping ice with ammonium fluoride ($NH_4F$) leads to the disappearance of ice II from the phase diagram (Shephard et al. 2018). $NH_4F$ has a hydrogen-disordering effect on ice (Salzmann et al. 2019), which means that in the case of ice II, the free energy is raised by such an amount that competing ~~and already~~ hydrogen-disordered phases become more stable. The $NH_4F$-doping experiment also illustrates that ice II is strictly topologically constrained since small amounts of dopant have such a dramatic effect. Since ice II occupies an important central region of the phase diagram, it has been argued that its unique properties, including its exceptionally long correlation length, could be regarded as the original anomaly in the $H_2O$ system (Shephard et al. 2018). In any case, the doping-induced disappearance of ice II was the first instance of a dopant being used to remove a phase from the phase diagram.

If ice II should be regarded as the 'odd one out' is ultimately a matter of perspective. Considering its stability as well as its hydrogen ordered and defect-free structure, it could be argued that it is an 'ideal' phase of ice and that the hydrogen-disordered phases with their dynamic and defective structures should be regarded as 'odd'.

## Ices III and IX: Chiral $H_2O$

Ice III occupies the smallest region of thermodynamic stability in the phase diagram between 0.22 and 0.34 GPa (Tammann 1900, Bridgman 1912, 1937). Its tetragonal unit cell with $P4_12_12$ space group symmetry contains 12 water molecules, two different oxygen sites, and three types of hydrogen bonds (McFarlan 1936, Kamb and Datta 1960, Kamb and Prakash 1968, Rabideau et al. 1968, La Placa and Hamilton

1973). The crystal structure includes five-, seven-, and eight-membered rings. An important structural feature are 4-fold spirals of hydrogen-bonded water molecules running in the *c* direction (*cf.* Fig. 3). These spirals can be either left- or right-handed which makes ice III a chiral phase of ice (Salzmann 2019). The enantiomorphic counterpart of $P4_12_12$ is $P4_32_12$. Ice III is less dense than ice II and it is isostructural with the $SiO_2$ polymorph keatite. Originally, ice III was believed to be completely hydrogen-disordered (Wilson et al. 1965, Whalley and Davidson 1965). However, *in situ* neutron diffraction showed that ice III is actually partially ordered with the occupancies of the hydrogen sites deviating from ½ (Londono et al. 1993, Kuhs et al. 1998, Lobban et al. 2000).

Upon cooling under pressure, ice III transforms to its anti-ferroelectric hydrogen-ordered counterpart ice IX between 208 and 165 K (Whalley et al. 1968). The ice III to IX phase transition is the only hydrogen-ordering phase transition in ice observed so far where the space group symmetry does not change. Unlike ice III, the dimensions of the unit cell of ice IX are close to cubic (La Placa and Hamilton 1973, Londono et al. 1993). In stark contrast to the "ice-nine" in Kurt Vonnegut's novel *Cat's Cradle* (Vonnegut 1963), which is a fictional stable form of ice at room temperature and ambient pressure, the real ice IX is metastable with respect to ice II below the region of stability of ice III (Petrenko and Whitworth 1999). Due to its metastability, ice IX is often found in sequences of phase transitions at low temperatures following Ostwald's rule of stages up to ~ 0.7 GPa (Salzmann et al. 2004a, Salzmann et al. 2008). Using single-crystal neutron diffraction, $D_2O$ ice IX was shown to contain a small amount of residual hydrogen order (La Placa and Hamilton 1973, Londono et al. 1993). Spectroscopic studies of ice IX samples at low temperatures and ambient pressure confirmed its highly hydrogen-ordered nature (Bertie and Bates 1977, Bertie and Francis 1982, Bertie et al. 1968a). The experimental ordered structure was confirmed to be the lowest energy structure with DFT calculations (Knight and Singer 2006).

The phase transition from ice III to ice IX upon cooling under pressure was followed with dielectric spectroscopy (Whalley et al. 1968), calorimetry (Nishibata and Whalley 1974), and Raman spectroscopy (Minceva-Sukarova et al. 1984). It was found that cooling rates greater than 1–2 K $min^{-1}$ are needed in order to suppress its transformation to the stable ice II (Minceva-Sukarova et al. 1984, Arnold et al. 1971). Upon heating, ice ~~XI~~ ~~always~~ transforms to ice II, which means that the ice IX to ice III phase transition has not been observed so far (Whalley et al. 1968, Nishibata and Whalley 1974, Minceva-Sukarova et al. 1984).

## Ices V and XIII: Structural Complexity at Its Most Extreme

Ice V is denser than ice II and its region of thermodynamic stability is found between 0.35 and 0.60 GPa (Tammann 1900, Bridgman 1912). Its monoclinic unit cell with $C2/c$ space group symmetry contains 28 water molecules, four distinct oxygen sites, and seven types of hydrogen bonds (Kamb et al. 1967, Hamilton et al. 1969). Four-, five-, six-, eight-, nine-, ten-, and twelve-membered rings exist within its structure illustrating the remarkable structural complexity of this phase of ice (*cf.* Fig. 3).

The structure can be described with two types of zigzag chains that run parallel to the *a* axis and form two layers within the unit cell. The hydrogen-disordered nature of ice V was demonstrated using dielectric spectroscopy (Wilson et al. 1965) and thermodynamic considerations (Whalley and Davidson 1965). The structural complexity of ice V also manifests in vibrational spectroscopy (Bertie and Whalley 1964b, Minceva-Sukarova et al. 1986, Tran et al. 2017). Using *in situ* neutron diffraction, it was shown that ice V is not fully hydrogen disordered with some of the fractional occupancies of the hydrogen sites deviating substantially from ½ (Kuhs et al. 1998, Lobban et al. 2000). Two of the hydrogen sites in *C*2/*c* are restricted to ½ occupancy which means that this space group does not allow full hydrogen order. Pure $H_2O$ ice V shows an orientational glass transition at ~ 130 K upon heating at ambient pressure at 30 K $min^{-1}$ corresponding to the unfreezing of reorientation dynamics of the water molecules (Salzmann et al. 2003a, Salzmann et al. 2011).

Weak hydrogen ordering upon cooling pure ice V has been suggested in several studies (Kamb and La Placa 1974, Minceva-Sukarova et al. 1988, Handa et al. 1988). Fully hydrogen-ordered ice V, which was named ice XIII, was obtained using hydrochloric acid (HCl) as a dopant and slow-cooling at ambient pressure (Salzmann et al. 2006c). The space group symmetry of the antiferroelectric ice XIII is $P2_1/a$ with seven distinct oxygen positions and 14 different hydrogen bonds which makes it by far the most structurally complicated phase of ice. During the ice V to ice XIII phase transition, the *a* lattice constant and the monoclinic angle $\beta$ increase whereas the *b* and *c* lattice constants contract (Salzmann et al. 2007).

Using calorimetry, it was shown that the ice V to ice XIII phase transition at ~ 113 K goes along with a 66% loss of Pauling entropy upon slow-cooling at ambient pressure (Salzmann et al. 2008). Considering the highly ordered nature of ice XIII, this value reflects the partially ordered nature of ice V. According to calorimetry, the ice V to ice XIII phase transition takes place in at least two overlapping stages (Salzmann et al. 2008). Slow-cooling under pressure gives a slightly more disordered ice XIII. The highly hydrogen-ordered nature of ice XIII can also be seen from its Raman spectrum (Salzmann et al. 2006a). The ice V to ice XIII phase transition has also been reproduced computationally (Knight and Singer 2008).

The role of the acid dopant is to produce mobile $H_3O^+$ point defects that speed up molecular reorientation dynamics and hence enable the hydrogen ordering phase transition to take place at low temperatures. The effect of HCl doping on the dielectric relaxation times was ~~recently~~ shown (Köster et al. 2016). Comparative studies of the effects of different acid dopants, such as HCl, HBr, $HClO_4$, and HF, on the hydrogen-ordering process during the ice V/XIII transition found that the interplay between acid strength and its solubility in ice determines the effectiveness of dopant with respect to enabling the hydrogen-ordering transition (Salzmann et al. 2008, Rosu-Finsen and Salzmann 2018). HF doping has an ordering effect on ice V but to a lesser extent than HCl which is the most effective hydrogen-ordering agent for ice V/XIII. Further studies into base dopants showed that LiOH facilitates the transition of ice V to ice XIII to the same extent as HF (Rosu-Finsen and Salzmann 2018). Therefore, ice XIII is the first hydrogen-ordered phase of ice that can be prepared with the help of both acid and base dopants.

## Ice IV: The Rule-breaker

The rule of numbering the phases of ice chronologically according to their dates of discovery was only broken once. Tammann suspected a metastable phase of ice to exist below the melting line of ice I*h* (Tammann 1910) which led Bridgman to skip the number IV when he discovered ice V (Bridgman 1912). Investigating the phase diagram of $D_2O$, Bridgman then identified a metastable phase which he named ice IV (Bridgman 1935). As far as we know, Bridgman's ice IV is different from the metastable phase originally suspected by Tammann. The metastable nature of ice IV is reflected in its challenging synthesis. After crystallization of liquid water to ice VI, ice IV is formed in the narrow window of 258.6–259.6 K and 0.500–0.535 GP a upon slow decompression of ice VI, taking care not to approach the melting pressure of ice VI (Nishibata 1972). The formation of ice IV following this route occurs only sporadically and in an unpredictable manner. However, organic nucleation agents have been successfully used to aid its formation (Evans 1967, Engelhardt and Whalley 1972). Due to its transient nature, ice IV has been called a "will-o'-the-wisp, ghostly form of ice" (Ball 1999). In a new approach, ice IV was prepared in a reproducible fashion by slowly heating high-density amorphous ice (HDA) at 0.81 GPa (Salzmann et al. 2002b, Salzmann et al. 2003c, Salzmann et al. 2004a).

Ice IV forms in a rhombohedral structure with 16 water molecules per unit cell (space group *R*-3*c*), two distinct oxygen sites, and four types of hydrogen bonds (Engelhardt and Kamb 1981, Klotz et al. 2003). The corresponding hexagonal cell contains 48 water molecules. The crystal structure features layers of puckered six-membered rings in a chair conformation that are interpenetrated by hydrogen bonds as shown in Fig. 3. The structure is in some sense similar to ice I but with hydrogen bonding between the second-nearest layers. In addition to the six-membered rings, eight- and ten-membered rings exist as well. Infrared and Raman spectroscopy suggest ice IV is hydrogen-disordered (Engelhardt and Whalley 1979, Salzmann et al. 2003b). At ambient pressure, $H_2O$ ice IV displays an orientational glass transition at ~ 140 K upon heating at 30 K $min^{-1}$ (Salzmann et al. 2004b). Recent molecular dynamics simulations of HDA identified local environments similar to those of ice IV and experimental comparisons with the isostructural $NH_4F$ phases suggested that HDA is a "derailed state" forming during the transition from ice I*h* to ice IV (Martelli et al. 2018, Shephard et al. 2017). Doping ice IV with HCl leads to the appearance of a weak endotherm in calorimetry around 113 K (Salzmann et al. 2011). ~~If~~ this feature arises as part of the kinetic unfreezing of molecular reorientation dynamics or ~~due to~~ the transition from a weakly hydrogen-ordered counterpart of ice IV is unclear (see question mark in Fig. 2). ~~The search for the hydrogen-ordered counterpart of ice IV certainly continues.~~

## Ices XII and XIV: Large Rings and Extreme Bending of Hydrogen Bonds

Another metastable polymorph, ice XII, forms in the stability domains of ices V and VI and was first prepared through slow crystallization of liquid water at 0.55 GPa (Lobban et al. 1998). The tetragonal ice XII structure (space group *I*-42*d*) contains

12 water molecules per unit cell with two distinct oxygen sites and two types of hydrogen bonds (Lobban et al. 1998, Koza et al. 1999). In the *a*-*b* projection, the ice XII structure resembles the Cairo tiling, which has five-membered rings only (Salzmann 2019). While such a two-dimensional phase of ice has been identified computationally (Chen et al. 2016), the ice XII structure actually contains seven- and eight-membered rings (O'Keeffe 1998) and is the densest known phase of ice without interpenetrating structural features. Instead, the high density is achieved by significant bending of the hydrogen bonds. In addition to the crystallization from the liquid, ice XII has been identified as an accidental byproduct during the preparation of HDA from ice I*h* at 77 K (Koza et al. 1999, Koza et al. 2000). Later, it was suggested that the ice XII formation is due to shock-wave heating (Kohl et al. 2001). Isobaric heating of HDA in the 0.7 to 1.4 GPa pressure range then revealed ice XII in mixtures with other crystalline polymorphs (Loerting et al. 2002). To prepare pure ice XII by heating HDA, it was shown that controlling the heating rate is crucial (for example > 11 K $min^{-1}$ at 0.8 GPa) (Salzmann et al. 2003c, Salzmann et al. 2004a).

Ice XII is fully hydrogen disordered as shown by neutron diffraction and Raman spectroscopy (Lobban et al. 1998, Salzmann et al. 2002a). Spectroscopically, ice XII appears to be very similar to a metastable phase discovered by Chou et al. (1998). However, if the Chou phase is indeed ice XII is still debated (Salzmann et al. 2004b, Yoshimura et al. 2007). Upon heating at ambient pressure, $H_2O$ ice XII displays an orientational glass transition at ~ 131 K upon heating at 30 K $min^{-1}$ (Salzmann et al. 2004b). Annealing below the glass transition temperature has been shown to produce kinetic overshoot effects (Salzmann et al. 2003a).

Doping ice XII with HCl leads to the formation of its hydrogen-ordered counterpart ice XIV below ~ 103 K (Salzmann et al. 2006c). Ice XIV is antiferroelectric and orthorhombic with $P2_12_12_1$ space group symmetry. Its unit cell contains three distinct oxygen sites and four types of hydrogen bonds. The reversibility of the ice XII to ice XIV phase transition at ambient pressure has been demonstrated (Salzmann et al. 2007, Salzmann et al. 2006b). However, cooling under pressure leads to a much more hydrogen-ordered ice XIV, which has been attributed to the pressure helping to overcome orthorhombic strain. The phase transition from ice XII to ice XIV goes along with expansions in the *a* and *c* lattice constants and a contraction in *b* (Salzmann et al. 2007). Doping with HF leads to less-ordered ice XIV (Köster et al. 2015), whereas KOH seems to be ineffective (Salzmann et al. 2006c). Following an initial claim of a complete release of Pauling entropy during the ice XII to ice XIV under pressure using HCl doping (Köster et al. 2015), an integration mistake of the calorimetric data was conceded and the value was corrected to 60% (Köster et al. 2018). If the effect of temperature is considered correctly upon integration, it has been argued that the actual value should be 51%, which means that ice XIV still contains significant amounts of hydrogen disorder (Rosu-Finsen and Salzmann 2018). The energetics of the ordering of ice XIV are consistent with DFT calculations (Tribello et al. 2006).

## Ices VI ~~and XV~~: Self-clathrates

Ice VI is stable between 0.6 and 2.2 GPa and the first of the high-pressure phases of ice to display a melting point greater than 0ºC (Bridgman 1912). For this reason, it

was nick-named "hot ice" (Walter 1990). Its tetragonal crystal structure with $P4_2/nmc$ space group symmetry contains 10 water molecules, two distinct oxygen sites, and three types of hydrogen bonds (*cf*. Fig. 3) (Kamb 1965). Furthermore, ice VI is the first of the high-pressure phases of ice to contain two independent and interpenetrating hydrogen-bonded networks. Ice VI has therefore been called a "self-clathrate" (Kamb 1965). The networks consist of hexameric units with structures like the $(H_2O)_6$ 'cage-like' cluster in the gas phase (Liu et al. 1996, Ludwig 2001). To build up a network, the hexameric units share corners in the *c* direction and are hydrogen-bonded to one another in the *a* and *b* directions. Ice VI is isostructural with the edingtonite $SiO_2$ polymorph (Kamb 1965). The $P4_2/nmc$ space group requires ice VI to be completely hydrogen disordered and its crystal structure was confirmed using *in situ* neutron diffraction (Kuhs et al. 1984, Kuhs et al. 1989). The hydrogen-disordered nature of ice VI is also consistent with dielectric (Wilson et al. 1965) and calorimetric measurements (Hobbs 1974). The *in situ* equation of state of ice VI has been measured using neutron diffraction (Fortes et al. 2012). The crystallization of ice VI from the liquid has been shown to be affected by the presence of sodium halides (Zeng et al. 2017, Zeng et al. 2016). Upon heating $H_2O$ ice VI at ambient pressure, an orientational glass transition is found at ~ 134 K (Shephard and Salzmann 2016).

The search for the hydrogen-ordered counterpart of ice VI began quite early. Kamb (1965) already mentioned the observation of a reflection in the X-ray diffraction of ice VI at 95 K and ambient pressure which is inconsistent with the reflection conditions of $P4_2/nmc$ (Kamb 1965) and he later assigned *Pmmn* space group symmetry to what he called ice VI' (Kamb 1973). *Pmmn* allows partial hydrogen order and implies antiferroelectric hydrogen ordering. However, this was not reproduced in later neutron diffraction work (Kuhs et al. 1984, Kuhs et al. 1989). Weak hydrogen ordering upon cooling ice VI under pressure has been suggested from dielectric (Johari and Whalley 1976, 1979), thermal conductivity (Ross et al. 1978), and thermal expansion measurements (Mishima et al. 1979). In contrast to Kamb's ice VI' (Kamb 1973), ~~the~~ dielectric measurements implied ferroelectric ordering of ice VI upon cooling under pressure (Johari and Whalley 1976, 1979). Raman and FT-IR spectroscopy of ice VI at low temperatures did not identify any signs of hydrogen order (Bertie et al. 1968b, Minceva-Sukarova et al. 1986), even when the sample was doped with KOH (Minceva-Sukarova et al. 1988).

Using HCl as a dopant led to the discovery of the antiferroelectric ice XV, the hydrogen-ordered counterpart of ice VI (Salzmann et al. 2009). The most ordered ice XV was obtained after slow-cooling at ambient pressure. Its pseudo-orthorhombic unit cell with *P*-1 space group symmetry contains five distinct oxygen sites and ten types of hydrogen bonds (Salzmann et al. 2009, Salzmann et al. 2016). There are three different ways in which the hexameric units can become hydrogen ordered. The experimental structure contains the most polar individual networks. However, the polarity of the networks is cancelled by the centrosymmetric *P*-1 space group symmetry (Salzmann et al. 2016). The antiferroelectric nature of ice XV is consistent with its Raman spectrum (Whale et al. 2013).

The phase transition from ice VI to ice XV starting at ~ 130 K at ambient pressure goes along with contractions in *a* and *b* whereas there is a significant expansion in *c* which leads to an overall volume expansion. The increase in volume upon hydrogen-

ordering explains why the most ordered states of ice XV are obtained upon cooling at ambient pressure. As can be seen from the changes in lattice constants but also calorimetric data, the ice VI to ice XV phase transition is quite fast at first, followed by a long tail so that the entire phase transition takes place over a ~ 30 K window (Shephard and Salzmann 2015, Salzmann et al. 2016). This rather large window has been explained with the complication that the ice VI to ice XV phase transitions must include the hydrogen-ordering of the individual networks as well as establishing ordering of the two networks with respect to one another. Even slow-cooling at ambient pressure only achieves a ~ 50% loss of the Pauling entropy. Recently, HCl was confirmed as the most effective dopant for making ice XV (Rosu-Finsen and Salzmann 2018). In addition to HF, doping with HBr also proved to enable hydrogen ordering. This was somewhat surprising since HBr doping is ineffective for preparing ice XIII. It was speculated that the large bromide anions could be accommodated within the ice VI/XV lattice by partially substituting one of the hexameric units and that this is not be possible for the more 'densely-knit ice' V/XIII network (Rosu-Finsen and Salzmann 2018).

In contrast to the experimental *P*-1 structure, DFT calculations suggested that the lowest energy ice XV structure is ferroelectric with *Cc* space group symmetry (Knight and Singer 2005, Kuo and Kuhs 2006). A later study using fragment-based 2nd order perturbation and coupled cluster theory then suggested the antiferroelectric *P*-1 structure as the lowest energy structure (Nanda and Beran 2013). This result was subsequently contested using the fully periodic 2nd order Møller-Plesset perturbation theory and the DFT random phase approximation reconfirming the original *Cc* structure (Del Ben et al. 2014). However, in this study it was also shown that the various possible ferroelectric structures can be destabilized by the dielectric properties of the surrounding medium. Hence, a mechanism by which antiferroelectric domains could become stabilized was identified providing an explanation for the apparent discrepancy between theory and experiment.

Upon increasing the pressure, the formation of ice XV becomes more and more difficult (Komatsu et al. 2016, Salzmann et al. 2016). For example, $D_2O$ samples either quenched at 1.0 GPa or slow-cooled at 1.4 GPa were identified as ice VI in neutron diffraction, and hence, lacking any significant hydrogen ordering. Heating such samples at ambient pressure revealed a 'transient' ordering feature both in neutron diffraction as well as in calorimetry which was followed by a phase transition to ice VI (Shephard and Salzmann 2015, Salzmann et al. 2016). The transient ordering feature can be explained by the high free energy of the essentially ice VI states and hence the strong tendency to hydrogen order at low pressures.

Slow-cooling HCl-doped ice VI at pressures greater than 1 GPa then brought about an irreversible endotherm upon heating at ~ 105 K preceding the transient ordering. This new low-temperature endotherm was initially attributed to a new hydrogen ordered phase of ice that was suggested to be more and differently hydrogen-ordered than ice XV (Gasser et al. 2018, Thoeny et al. 2019). Furthermore, a strong isotope effect was suggested that prevents the formation of a corresponding $D_2O$ phase. In response to this, it was suggested that the new low-temperature endotherm is related to the glass transition of 'deep-glassy' states of ice VI (Rosu-Finsen and Salzmann 2019, Rosu-Finsen et al. 2020). It was shown that the low-temperature

endotherms displayed all the characteristics of endothermic overshoot effects related to a glass transition. This included a typical dependence on pressure and cooling rate, the fact that they could be produced by sub-$T_g$ annealing at ambient pressure and that they could be made to appear or disappear depending on the heating rate and the initial extent of relaxation. Such deep glassy states have been observed for a variety of other materials (Moynihan et al. 1976, Zhao et al. 2013). Furthermore, deep-glassy states of ice VI were also identified for corresponding $D_2O$ samples and the proposed deep-glassy ice VI scenario was shown to be consistent with X-ray diffraction recorded by Gasser et al. (Rosu-Finsen and Salzmann 2019). Further to this, using a combination of neutron spectroscopy and diffraction, an HCl-doped $H_2O$ deep-glassy ice VI sample was compared with pure ice VI and ice XV (Rosu-Finsen et al. 2020). This showed that deep-glassy ice VI is very closely related to ice VI from both the spectroscopic as well as the diffraction point of view (Rosu-Finsen et al. 2020). Additionally, in line with expectation, it has been shown that the hydrogen-ordered structure of $D_2O$ ice XV can be used to ~~analyze~~ the corresponding $H_2O$ phase.

## Ices VII, VIII, X, and XVIII: the High-pressure Frontier

Ice VII is a stable phase of ice above 2.1 GPa (Bridgman 1937, Pistorius et al. 1968). Like ice VI, it contains two interpenetrating networks that are isostructural with ice I*c* (Kuhs et al. 1984, Jorgensen and Worlton 1985). Its cubic unit cell with *Pn*-3*m* space group symmetry contains two water molecules, one distinct oxygen site, and one type of hydrogen bond (*cf*. Fig. 3). The *Pn*-3*m* space group requires ice VII to be completely hydrogen disordered. In addition to ice I*h*, ice VII is the second phase of ice considered to be a mineral following its discovery as an inclusion compound inside diamonds (Tschauner et al. 2018). Due to its simple structure, ice VII has been a testbed for probing the positional disorder of the oxygen atoms induced by the hydrogen-disorder (Kuhs et al. 1984, Jorgensen and Worlton 1985, Nelmes et al. 1998, Knight and Singer 2009, Bellin et al. 2011). In a recent neutron diffraction study, ice VII has been compressed beyond 60 GPa (Guthrie et al. 2019). In contrast to ice I*h*, ice VII can accommodate lithium chloride and bromide at ~ 1:6 LiX:$H_2O$ molar ratios (Klotz et al. 2016, Klotz et al. 2009). The unit cell volume of 'salty' ice VII is strongly increased and the concomitant positional disorder of $H_2O$ makes it a "plastic" phase of ice. Compared to the lithium halides, the solubility of NaCl in ice VII is much smaller (Ludl et al. 2017).

Upon cooling, ice VII transforms to its hydrogen-ordered counterpart ice VIII within a narrow temperature range around 273 K over quite a large pressure range (Whalley et al. 1966, Pistorius et al. 1968, Johari et al. 1974). In addition to the ice III to ice IX phase transition, this is the only other hydrogen ordering phase transition that takes place without the help of dopants. ~~Furthermore, the ice VII to ice VIII phase transition is the only case reported so far where the size of the unit cell changes upon hydrogen ordering.~~ The ice VIII unit cell is tetragonal with $I4_1/amd$ space group symmetry ($a_{VIII} = \sqrt{2}a_{VII}$ *and* $c_{VIII} = 2a_{VII}$) (Jorgensen et al. 1984, Kuhs et al. 1984). Similar to the situation for ice XV, the two networks in ice VIII are as polar as they can be but because of the $I4_1/amd$ space group symmetry, the

polarities of the individual networks are cancelled so that ice VIII is antiferroelectric overall. Recent *in situ* neutron diffraction work has shown that the ice VII to ice VIII phase transitions slows down around 10 GPa but then becomes fast again at higher pressures (Komatsu et al. 2020a). These findings have been attributed to a crossover in the hydrogen dynamics and several of the previously observed anomalies of ice VII in this pressure range (Okada et al. 2014, Noguchi and Okuchi 2016, Hirai et al. 2014) have been attributed to this phenomenon. Furthermore, the hydrogen ordering of ice VII can be slowed down and partially prevented by using $NH_4F$ as a dopant (Salzmann et al. 2019). Close to completely hydrogen-disordered ice VII can be obtained by low temperature compression of HDA or ice VI to make a phase of ice called ice VII' (Hemley et al. 1989, Klotz et al. 1999).

Recovered at ambient pressure, ices VII' and VIII behave differently to the other high-pressure phases of ice upon heating. Instead of transforming to ice I*sd*, they form low-density amorphous ice (LDA) first (Klug et al. 1989, Klotz et al. 1999, Klotz et al. 2005). Using Raman spectroscopy and X-ray diffraction, the LDA from ice VIII was shown to be different compared to other types of LDA formed through, for example, vapor deposition onto a cold substrate (Shephard et al. 2016).

Compression of ice VII beyond 60 GPa leads to the formation of cubic ice X with *Pn*-3*m* space group symmetry (Stillinger and Schweitzer 1983, Polian and Grimsditch 1984, Aoki et al. 1996, Teixeira 1998, Goncharov et al. 1996, Goncharov et al. 1999). The hydrogen atoms in ice X are located halfway between the oxygen atoms which means that the water molecules lose their molecular character as shown in Fig. 1b. Experimentally, it has been shown that ice X persists up to at least 210 GPa (Goncharov et al. 1996). However, recent *in situ* Raman measurements have suggested that the transition from ice VII to ice X may not actually occur below 120 GPa (Zha et al. 2016). Furthermore, incorporating LiCl into ice VII has been shown to shift the phase transition from ice VII to ice X towards higher pressures (Bove et al. 2015). A variety of post-ice X phases have been predicted computationally (Benoit et al. 1996, Militzer and Wilson 2010, Pickard et al. 2013).

Subjecting ice VII to sophisticated laser-driven shock-compression, superionic ice XVIII with *Fm*-3*m* space group symmetry forms above 100 GPa and 2000 K (Millot et al. 2018, Millot et al. 2019). The hydrogen atoms in ice XVIII are free to move between the densely packed oxygen atoms. Ice XVIII has a melting point near 5000 K at 190 GPa which means that it may be present in the interiors of Neptune and Uranus. A variety of other superionic ices have been predicted computationally (Sun et al. 2015).

## Ices XVI and XVII: The Empty Clathrate Hydrates

Two low-density ices can be accessed from the corresponding gas clathrate hydrates. Several hundreds of hypothetical structures have been explored by computational efforts in the search for new ice modifications, but hitherto, only two have been realized experimentally (Kosyakov and Shestakov 2001, Matsui et al. 2017, Huang et al. 2016, Huang et al. 2017).

A neon clathrate hydrate with the cubic structure II can be formed by pressurizing ice I*h* to 0.35 GPa at 244 K. By pumping the material to low pressures, the neon atoms

~~can~~ escape the cages in the clathrate structure, leaving behind the empty clathrate hydrate structure, which was named ice XVI (Falenty et al. 2014). Hydrogen-disordered ice XVI contains 136 water molecules and three distinct oxygen sites in its cubic unit cell with *Fd*-3*m* space group symmetry. The hydrogen bonds form two types of empty cages as shown in Fig. 3. These cages consist of five- and six-membered rings. The removal of neon from the cages during formation leads to a volume increase, resulting in a density of 0.81 g cm$^{-3}$ (Falenty et al. 2014). Recently, refilling of the clathrate cages in ice XVI with helium led to the first reported helium clathrate hydrate (Kuhs et al. 2018).

In a similar approach, a hydrogen-filled ice structure was first prepared by exposing ice to ~ 0.4 GPa of $H_2$ gas at 255 K (Strobel et al. 2016). By pumping the material at 120 K, hydrogen can be reversibly extracted from the clathrate hydrate with $C_0$-type structure to obtain the empty clathrate named ice XVII (del Rosso et al. 2016a). Reducing the $H_2$ content causes a decrease of the lattice parameter *c*, but an increase of *a*. The water molecules in the hexagonal unit cell of ice XVII with space group $P6_122$ (or $P6_522$) and one distinct oxygen site form a network of five-membered rings. This gives rise to interconnected spiral chains around spacious hexagonal channels in the overall hydrogen-disordered structure (del Rosso et al. 2016b). In addition to ices III/IX, ice XVII displays a second type of chiral ice structure. This type of structure was also recently found for a $CO_2$ clathrate hydrate (Amos et al. 2017).

## Conclusions

The exploration of water's phase diagram started more than a century ago with the work of Tammann and Bridgman (Tammann 1900, 1910, Bridgman 1912). Starting with the development of piston cylinders to the modern-day laser shock-wave heating experiments, new experimental techniques have always been tested with respect to exploring the phase diagram of $H_2O$ to ever higher pressures and temperatures, and there is no doubt that this trend will continue in the future. In addition to exploring extreme pressure and temperature conditions, the last decade has seen a new trend emerging with a large number of studies exploring the 'chemical' dimension of ice research. This has included work on enabling hydrogen ordering with the help of dopants, using small gas species as removable templates for growing low-density ice phases, the formation of 'salty' ices with very high concentrations of dissolved species and the selective disappearance of a phase of ice with the help of an impurity. Knowing how ice behaves when mixed with other chemical species is of course highly relevant for environmental research and the vast research area of clathrate hydrates (Ripmeester et al. 2006, Loveday and Nelmes 2008). Interestingly, working on this review we also realized that the intermediate pressure range, which includes ices III, V, and II and their (dis)ordered counterparts, has actually not received as much attention as the exploration of the higher-pressure phases. In any case, the $H_2O$ system will without doubt reveal many more secrets in the future and we can only wonder what the next phase of ice will be.

## References

Amaya, A. J., H. Pathak, V. P. Modak, H. Laksmono, N. D. Loh, J. A. Sellberg et al. 2017. How cubic can ice be? J. Chem. Phys. Lett. 8: 3216–3222.

Amos, D. M., M.-E. Donnelly, P. Teeratchanan, C. L. Bull, A. Falenty, W. F. Kuhs et al. 2017. A chiral gas–hydrate structure common to the carbon dioxide–water and hydrogen–water systems. J. Phys. Chem. Lett. 8: 4295–4299.

Aoki, K., H. Yamawaki, M. Sakashita and H. Fujihisa. 1996. Infrared absorption study of the hydrogen-bond symmetrization in ice to 110 GPa. Phys. Rev. B 54: 15673–15677.

Aragones, J. L. and C. Vega. 2009. Plastic crystal phases of simple water models. J. Chem. Phys. 130: 244504.

Arakawa, M., H. Kagi, J. A. Fernandez-Baca, B. C. Chakoumakos and H. Fukazawa. 2011. The existence of memory effect on hydrogen ordering in ice: the effect makes ice attractive. Geophys. Res. Lett. 38: L16101.

Arnold, G. P., R. G. Wenzel, S. W. Rabideau, N. G. Nereson and A. L. Bowman. 1971. Neutron diffraction study of ice polymorphs under helium pressure. J. Chem. Phys. 55: 589–595.

Ball, P. 1999. $H_2O$ A Biography of Water: Weidenfeld & Nicolson.

Barnes, W. H. and W. H. Bragg. 1929. The crystal structure of ice between 0ºC and –183ºC. Proc. Roy. Soc. A125: 670–693.

Bellin, C., B. Barbiellini, S. Klotz, T. Buslaps, G. Rousse, T. Strässle et al. 2011. Oxygen disorder in ice probed by x-ray Compton scattering. Phys. Rev. B 83: 094117.

Benoit, M., M. Bernasconi, P. Rocher and M. Parrinello. 1996. New high-pressure phase of ice. Phys. Rev. Lett. 76: 2934–2936.

Bernal, J. D. and R. H. Fowler. 1933. A theory of water and ionic solution, with particular reference to hydrogen and hydroxyl ions. J. Chem. Phys. 1: 515–549.

Bertie, J. E. and E. Whalley. 1964a. Infrared Spectra of Ices I*h* and I*c* in the Range 4000 to 350 $cm^{-1}$. J. Chem. Phys. 40: 1637–1645.

Bertie, J. E. and E. Whalley. 1964b. Infrared spectra of ices II, III, and V in the range 4000 to 350 $cm^{-1}$. J. Chem. Phys. 40: 1646–1659.

Bertie, J. E., H. J. Labbé and E. Whalley. 1968a. Far-infrared spectra of ice II, V, and IX. J. Chem. Phys. 49: 775–780.

Bertie, J. E., H. J. Labbé and E. Whalley. 1968b. Infrared Spectrum of Ice VI in the Range 4000–50 $cm^{-1}$. J. Chem. Phys. 49: 2141–2144.

Bertie, J. E. and F. E. Bates. 1977. Mid-infrared spectra of deuterated ices at 10°K and interpretation of the OD stretching bands of ices II and IX. J. Chem. Phys. 67: 1511–1518.

Bertie, J. E. and B. F. Francis. 1980. Raman spectra of the O-H and O-D stretching vibrations of ice II and IX to 25°K at atmospheric pressure. J. Chem. Phys. 72: 2213–2221.

Bertie, J. E. and B. F. Francis. 1982. Raman spectra of ices II and IX above 35 K at atmospheric pressure: translational and rotational vibrations. J. Chem. Phys. 77: 1–15.

Bove, L. E., R. Gaal, Z. Raza, A.-A. Ludl, S. Klotz, A. M. Saitta et al. 2015. Effect of salt on the H-bond symmetrization in ice. Proc. Natl. Acad. Sci. USA 112: 8216–8220.

Bragg, S. W. H. 1921. The crystal structure of ice. Proc. Phys. Soc. 34: 98–103.

Bridgman, P. W. 1912. Water, in the liquid and five solid forms under pressure. Proc. Am. Acad. Arts Sci. 47: 441–558.

Bridgman, P. W. 1935. The pressure-volume-temperature relations of the liquid, and the phase diagramm of heavy water. J. Chem. Phys. 3: 597–605.

Bridgman, P. W. 1937. The phase diagramm of water to 45000 $kg/cm^2$. J. Chem. Phys. 5: 964–966.

Carr, T. H. G., J. J. Shephard and C. G. Salzmann. 2014. Spectroscopic signature of stacking disorder in ice I. J. Phys. Chem. Lett. 5: 2469–2473.

Chen, J., G. Schusteritsch, C. J. Pickard, C. G. Salzmann and A. Michaelides. 2016. Two dimensional ice from first principles: Structures and phase transitions. Phys. Rev. Lett. 116: 025501.

Chou, I.-M., J. G. Blank, A. F. Goncharov, H.-K. Mao and R. J. Hemley. 1998. *In situ* observations of a high-pressure phase of $H_2O$ ice. Science 281: 809–812.

Del Ben, M., J. VandeVondele and B. Slater. 2014. Periodic MP2, RPA, and boundary condition assessment of hydrogen ordering in ice XV. J. Phys. Chem. Lett. 5: 4122–4128.

del Rosso, L., M. Celli and L. Ulivi. 2016a. New porous water ice metastable at atmospheric pressure obtained by emptying a hydrogen-filled ice. Nat. Comm. 7: 13394.

del Rosso, L., F. Grazzi, M. Celli, D. Colognesi, V. Garcia-Sakai and L. Ulivi. 2016b. Refined structure of metastable ice XVII from neutron diffraction measurements. J. Phys. Chem. C 120: 26955–26959.

del Rosso, L., M. Celli, F. Grazzi, M. Catti, T. C. Hansen, A. D. Fortes et al. 2020. Cubic ice I*c* without stacking defects obtained from ice XVII. Nat. Mat.: https://doi.org/10.1038/s41563-020-0606-y.

Dennison, D. M. 1921. The crystal structure of ice. Phys. Rev. 17: 20–22.

Durham, W. B., S. H. Kirby and L. A. Stern. 1997. Creep of water ices at planetary conditions: A compilation. J. Geophys. Res. 102: 16293–16302.

Dyadin, Y. A., E. G. Larionov, E. Y. Aladko, A. Y. Manakov, F. V. Zhurko, T. V. Mikina et al. 1999. Clathrate formation in water-noble gas (Hydrogen) systems at high pressures. J. Struct. Chem. 40: 790–795.

Echelmeyer, K. and B. Kamb. 1986. Rheology of ice II and ice III from high-pressure extrusion. Geophys. Res. Lett. 13: 693–696.

Engelhardt, H. and E. Whalley. 1972. Ice IV. J. Chem. Phys. 56: 2678–2684.

Engelhardt, H. and E. Whalley. 1979. The infrared spectrum of ice IV in the range 4000–400 $cm^{-1}$. J. Chem. Phys. 71: 4050–4051.

Engelhardt, H. and B. Kamb. 1981. Structure of Ice IV, a Metastable High-pressure Phase. J. Chem. Phys. 75: 5887–5899.

Evans, L. F. 1967. Selective nucleation of the high-pressure ices. J. Appl. Phys. 38: 4930–4932.

Falenty, A., T. C. Hansen and W. F. Kuhs. 2014. Formation and Properties of Ice XVI Obtained by Emptying a Type sII Clathrate Hydrate. Nature 516: 231–233.

Finch, E. D., S. W. Rabideau, R. G. Wenzel and N. G. Nereson. 1968. Neutron-diffraction study of ice polymorphs. II. Ice II. J. Chem. Phys. 49: 4361–4365.

Finney, J. L. 2001. The water molecule and its interactions: the interaction between theory, modelling, and experiment. J. Mol. Liq. 90: 303–312.

Fortes, A. D., I. G. Wood, J. P. Brodholt and L. Vočadlo. 2003. *Ab initio* simulation of the ice II structure. J. Chem. Phys. 119: 4567–4572.

Fortes, A. D., I. G. Wood, M. Alfredsson, L. Vocadlo and K. S. Knight. 2005. The incompressibility and thermal expansivity of $D_2O$ ice II determined by powder neutron diffraction. J. Appl. Crystal. 38: 612–618.

Fortes, A. D., I. G. Wood, M. G. Tucker and W. G. Marshall. 2012. The P-V-T equation of state of $D_2O$ ice VI determined by neutron powder diffraction in the range $0 < P < 2.6$ GPa and $120 < T < 330$ K, and the isothermal equation of state of $D_2O$ ice VII from 2 to 7 GPa at room temperature.

Fortes, A. D. 2018. Accurate and precise lattice parameters of $H_2O$ and $D_2O$ Ice I*h* between 1.6 and 270 K from high-resolution time-of-flight neutron powder diffraction data. Acta Cryst. B74: 196–216.

Fortes, A. D. 2019. Structural manifestation of partial proton ordering and defect mobility in ice I*h*. Phys. Chem. Chem. Phys. 21: 8264–8274.

Fukazawa, H., A. Hoshikawa, H. Yamauchi, Y. Yamaguchi and Y. Ishii. 2005. Formation and Growth of ice XI: A Powder Neutron Diffraction Study. J. Crystal Growth 282: 251–259.

Fukazawa, H., A. Hoshikawa, Y. Ishii, B. C. Chakoumakos and J. A. Fernandez-Baca. 2006. Existence of Ferroelectric Ice in the Universe. Astrophys. J. 652: L57–L60.

Gasser, T. M., A. V. Thoeny, L. J. Plaga, K. W. Köster, M. Etter, R. Böhmer et al. 2018. Experiments indicating a second hydrogen ordered phase of ice VI. Chem. Sci. 9: 4224–4234.

Goncharov, A. F., V. V. Struzhkin, M. S. Somayazulu, R. J. Hemley and H. K. Mao. 1996. Compression of ice to 210 gigapascals: Infrared evidence for a symmetric hydrogen-bonded phase. Science 273: 218–220.

Goncharov, A. F., V. V. Struhkin, M. Ho-kwang and R. J. Hemley. 1999. Raman spectroscopy of dense $H_2O$ and the transition to symmetric hydrogen bonds. Phys. Rev. Lett. 83: 1998–2001.

Gupta, M. K., R. Mittal, B. Singh, S. K. Mishra, D. T. Adroja, A. D. Fortes et al. 2018. Phonons and anomalous thermal expansion behavior of $H_2O$ and $D_2O$ ice I*h*. Phys. Rev. B 98: 104301.

Guthrie, M., R. Boehler, J. J. Molaison, B. Haberl, A. M. dos Santos and C. Tulk. 2019. Structure and disorder in ice VII on the approach to hydrogen-bond symmetrization. Phys. Rev. B 99: 184112.

Hamilton, W. C., B. Kamb, S. J. La Placa and A. Prakash. 1969. *In*: Riehl, N., B. Bullemer and H. Engelhardt (eds.). Physics of Ice. New York: Plenum.

Handa, Y. P., D. D. Klug and E. Whalley. 1986. Difference in energy between cubic and hexagonal ice. J. Chem. Phys. 84: 7009–7010.

Handa, Y. P., D. D. Klug and E. Whalley. 1988. Energies of the phases of ice at low temperature and pressure relative to ice I*h*. Can. J. Chem. 66: 919–924.

Hansen, T. C., M. M. Koza and W. F. Kuhs. 2008. Formation and annealing of cubic ice: I. modelling of stacking faults. J. Phys.: Condens. Matter 20: 285104.

Hemley, R. J., L. C. Chen and H. K. Mao. 1989. New transformations between crystalline and amorphous ice. Nature 338: 638–640.

Hernandez, J. A. and R. Caracas. 2018. Proton dynamics and the phase diagram of dense water ice. J. Chem. Phys. 148: 214501.

Hirai, H., H. Kadobayashi, T. Matsuoka, Y. Ohishi and Y. Yamamoto. 2014. High pressure X-ray diffraction and Raman spectroscopic studies of the phase change of D2O ice VII at approximately 11 GPa. High Pressure Res. 34: 289–296.

Hobbs, P. V. 1974. Ice Physics. Oxford: Clarendon Press.

Howe, R. and R. W. Whitworth. 1989. A determination of the crystal structure of ice XI. J. Chem. Phys. 90: 4450–4453.

Huang, Y., C. Zhu, L. Wang, X. Cao, Y. Su, X. Jiang et al. 2016. A new phase diagram of water under negative pressure: The rise of the lowest-density clathrate s-III. Sci. Adv. 2.

Huang, Y., C. Zhu, L. Wang, J. Zhao and X. C. Zeng. 2017. Prediction of a new ice clathrate with record low density: A potential candidate as ice XIX in guest-free form. Chem. Phys. Lett. 671: 186–191.

Jackson, S. M., V. M. Nield, R. W. Whitworth, M. Oguro and C. C. Wilson. 1997. Single-crystal neutron diffraction studies of the structure of ice XI. J. Phys. Chem. B 101: 6142–6145.

Johari, G. P., A. Lavergne and E. Whalley. 1974. Dielectric properties of ice VII and VIII and the phase boundary between ice VI and VII. J. Chem. Phys. 61: 4292–4300.

Johari, G. P. and E. Whalley. 1976. Dielectric properties of ice VI at low temperatures. J. Chem. Phys. 64: 4484–4489.

Johari, G. P. and E. Whalley. 1979. Evidence for a very slow transformation in ice VI at low temperatures. J. Chem. Phys. 70: 2094–2097.

Johari, G. P. 1998. An interpretation for the thermodynamic features of ice Ih<->ice XI transformation. J. Chem. Phys. 109: 9543–9548.

Jorgensen, J. D., R. A. Beyerlein, N. Watanabe and T. G. Worlton. 1984. Structure of $D_2O$ ice VIII from in situ powder neutron diffraction. J. Chem. Phys. 81: 3211–3214.

Jorgensen, J. D. and T. G. Worlton. 1985. Disordered structure of D2O ice VII from *in-situ* neutron powder diffraction. J. Chem. Phys. 83: 329–333.

Journaux, B., J. M. Brown, A. Pakhomova, I. E. Collings, S. Petitgirard, P. Espinoza et al. 2020. Holistic approach for studying planetary hydrospheres: Gibbs representation of ices thermodynamics, elasticity, and the water phase diagram to 2,300 MPa. J. Geophys. Res. 125: e2019JE006176.

Kamb, B. 1964. Ice II: A proton-ordered form of ice. Acta Cryst. 17: 1437–1449.

Kamb, B. 1965. Structure of ice VI. Science 150: 205–209.

Kamb, B., A. Prakash and C. Knobler. 1967. Structure of ice V. Acta Cryst. 22: 706–715.

Kamb, B. and A. Prakash. 1968. Structure of ice III. Acta Cryst. B24: 1317–1327.

Kamb, B., W. C. Hamilton, S. J. La Placa and A. Prakash. 1971. Ordered proton configuration in ice II, from single-crystal neutron diffraction. J. Chem. Phys. 55: 1934–1945.

Kamb, B. 1973. Crystallography of Ice. *In*: Whalley, E., S. J. Jones and L. W. Gold (eds.). Physics and Chemistry of Ice. Royal Society of Canada.

Kamb, B. and S. J. La Placa. 1974. Reversible order-disorder transformation in ice V. Trans. Am. Geophys. Union 56: 1202.

Kamb, W. B. and S. K. Datta. 1960. Crystal structures of the high-pressure forms of ice: Ice III. Nature 187: 140E.141.

Klotz, S., J. M. Besson, G. Hamel, R. J. Nelmes, J. S. Loveday and W. G. Marshall. 1999. Metastable ice VII at low temperature and ambient pressure. Nature 398: 681E.684.

Klotz, S., G. Hamel, J. S. Loveday, R. J. Nelmes and M. Guthrie. 2003. Recrystallisation of HDA ice under pressure by *in-situ* neutron diffraction to 3.9 GPa. Z. Kristallogr. 218: 117–122.

Klotz, S., T. Strässle, C. G. Salzmann, J. Philippe and S. F. Parker. 2005. Incoherent inelastic neutron scattering measurements on ice VII: Are there two kinds of hydrogen bonds in ice? Europhys. Lett. 72: 576–582.

Klotz, S., L. E. Bove, T. Strässle, T. C. Hansen and A. M. Saitta. 2009. The preparation and structure of salty ice VII under pressure. Nat. Mat. 8: 405–409.

Klotz, S., K. Komatsu, F. Pietrucci, H. Kagi, A. A. Ludl, S. Machida et al. 2016. Ice VII from aqueous salt solutions: From a glass to a crystal with broken H-bonds. Sci. Rep. 6: 32040.

Klug, D. D., Y. P. Handa, J. S. Tse and E. Whalley. 1989. Transformation of ice VIII to amorphous ice by "Melting" at low temperature. J. Chem. Phys. 90: 2390–2392.

Knight, C. and S. J. Singer. 2005. Prediction of a phase transition to a hydrogen bond ordered form of ice VI. J. Phys. Chem. B 109: 21040–21046.

Knight, C. and S. J. Singer. 2006. A reexamination of the ice III/IX hydrogen bond ordering phase transition. J. Chem. Phys. 125: 064506.

Knight, C. and S. J. Singer. 2008. Hydrogen bond ordering in ice V and the transition to ice XIII. J. Chem. Phys. 129: 164513.

Knight, C. and S. J. Singer. 2009. Site disorder in Ice VII arising from hydrogen bond fluctuations. J. Phys. Chem. A 113: 12433–12438.

Kohl, I., E. Mayer and A. Hallbrucker. 2001. Ice XII forms on compression of hexagonal ice at 77 K via high-density amorphous water. Phys. Chem. Chem. Phys. 3: 602–605.

Komatsu, K., F. Noritake, S. Machida, A. Sano-Furukawa, T. Hattori, R. Yamane et al. 2016. Partially Ordered State of Ice XV. Sci. Rep. 6: 28920.

Komatsu, K., S. Klotz, S. Machida, A. Sano-Furukawa, T. Hattori and H. Kagi. 2020a. Anomalous hydrogen dynamics of the ice VII–VIII transition revealed by high-pressure neutron diffraction. Proc. Natl. Acad. Sci. USA 117: 6356–6361.

Komatsu, K., S. Machida, F. Noritake, T. Hattori, A. Sano-Furukawa, R. Yamane et al. 2020b. Ice Ic without stacking disorder by evacuating hydrogen from hydrogen hydrate. Nat. Comm. 11: 464.

König, H. 1943. Eine kubische Eismodifikation. Z. Kristallogr. 105: 279–286.

Köster, K. W., V. Fuentes-Landete, A. Raidt, M. Seidl, C. Gainaru, T. Loerting et al. 2015. Dynamics enhanced by HCl doping triggers full Pauling entropy release at the ice XII–XIV transition. Nat. Comm. 6: 7349.

Köster, K. W., A. Raidt, V. Fuentes Landete, C. Gainaru, T. Loerting and R. Böhmer. 2016. Doping-enhanced dipolar dynamics in ice V as a precursor of hydrogen ordering in ice XIII. Phys. Rev. B 94: 184306.

Köster, K. W., V. Fuentes-Landete, A. Raidt, M. Seidl, C. Gainaru, T. Loerting et al. 2018. Author Correction: Dynamics enhanced by HCl doping triggers 60% Pauling entropy release at the ice XII–XIV transition. Nat. Comm. 9: 16189.

Kosyakov, V. I. and V. A. Shestakov. 2001. On the possibility of the existence of a new ice phase under negative pressures. Dokl. Phys. Chem. 376: 49–51.

Koza, M., H. Schober, A. Tölle, F. Fujara and T. Hansen. 1999. Formation of ice XII at different conditions. Nature 397: 660–661.

Koza, M. M., H. Schober, T. Hansen, A. Tölle and F. Fujara. 2000. Ice XII in its second regime of metastability. Phys. Rev. Lett. 84: 4112–4115.

Kuhs, W. F. and M. S. Lehmann. 1983. The structure of ice Ih by neutron diffraction. J. Phys. Chem. 87: 4312–4313.

Kuhs, W. F., J. L. Finney, C. Vettier and D. V. Bliss. 1984. Structure and hydrogen ordering in ices VI, VII, and VIII by neutron powder diffraction. J. Chem. Phys. 81: 3612–3623.

Kuhs, W. F., D. V. Bliss and J. L. Finney. 1987. High-resolution neutron powder diffraction study of ice $I_c$. J. Phys. Colloq., C1 48: 631–636.

Kuhs, W. F., H. Ahsbahs, D. Londono and J. L. Finney. 1989. *In-situ* crystal growth and neutron four-circle diffractometry under high pressure. Physica B 156–157: 684–687.

Kuhs, W. F., C. Lobban and J. L. Finney. 1998. Partial h-ordering in high pressure ices III and V. Rev. High Pressure Sci. Technol. 7: 1141–1143.

Kuhs, W. F., C. Sippel, A. Falentya and T. C. Hansen. 2012. Extent and Relevance of Stacking Disorder in "Ice I*c*". Proc. Natl. Acad. Sci. USA 109: 21259–21264.

Kuhs, W. F., T. C. Hansen and A. Falenty. 2018. Filling ices with helium and the formation of helium clathrate hydrate. J. Phys. Chem. Lett. 9: 3194–3198.

Kuo, J.-L. and W. F. Kuhs. 2006. A first principles study on the structure of ice-vi: Static distortion, molecular geometry, and proton ordering. J. Phys. Chem. B 110: 3697–3703.

La Placa, S. J. and W. C. Hamilton. 1973. On a nearly proton-ordered structure for ice IX. J. Chem. Phys. 58: 567–580.

Leadbetter, A. J., R. C. Ward, J. W. Clark, P. A. Tucker, T. Matsuo and H. Suga. 1985. The equilibrium low-temperature structure of ice. J. Chem. Phys. 82: 424–428.

Li, J.-C., J. D. Londono and D. K. Ross. 1991. An inelastic incoherent neutron scattering study of ice II, IX, V, and VI—in the range from 2 to 140 meV. J. Chem. Phys. 94: 6770–6775.

Line, C. M. B. and R. W. Whitworth. 1996. A high resolution neutron powder diffraction study of $D_2O$ ice XI. J. Chem. Phys. 104: 10008–10013.

Liu, K., M. G. Brown, C. Carter, R. J. Saykally, J. K. Gregory and D. C. Clary. 1996. Characterization of a cage form of the water hexamer. Nature 381: 501–503.

Lobban, C., J. L. Finney and W. F. Kuhs. 1998. The structure of a new phase of ice. Nature 391: 268–270.

Lobban, C., J. L. Finney and W. F. Kuhs. 2000. The structure and ordering of ices III and V. J. Chem. Phys. 112: 7169–7180.

Lobban, C., J. L. Finney and W. F. Kuhs. 2002. The p-T dependency of the ice II crystal structure and the effect of helium inclusion. J. Chem. Phys. 117: 3928–3834.

Loerting, T., I. Kohl, C. Salzmann, E. Mayer and A. Hallbrucker. 2002. The (Meta-)stability domain of ice XII revealed between ca. 158 - 212 K and ca. 0,7 - 1,5 GPa on isobaric heating of high density amorphous water. J. Chem. Phys. 116: 3171–3174.

Londono, D., J. L. Finney and W. F. Kuhs. 1992. Formation, stability, and structure of helium hydrate at high pressure. J. Chem. Phys. 97: 547–552.

Londono, J. D., W. F. Kuhs and J. L. Finney. 1993. Neutron diffraction studies of ices III and IX on under-pressure and recovered samples. J. Chem. Phys. 98: 4878–4888.

Loveday, J. S. and R. J. Nelmes. 2008. High-pressure gas hydrates. Phys. Chem. Chem. Phys. 10: 937–950.

Ludl, A. A., L. E. Bove, D. Corradini, A. M. Saitta, M. Salanne, C. L. Bull et al. 2017. Probing ice VII crystallization from amorphous NaCl–D2O solutions at gigapascal pressures. Phys. Chem. Chem. Phys. 19: 1875–1883.

Ludwig, R. 2001. Water: from clusters to the bulk. Angew. Chem. Int. Ed. 40: 1808–1827.

Malkin, T. L., B. J. Murray, A. V. Brukhno, A. J. and C. G. Salzmann. 2012. Structure of ice crystallized from supercooled water. Proc. Natl. Acad. Sci. USA 109: 1041–1045.

Malkin, T. L., B. J. Murray, C. G. Salzmann, V. Molinero, S. J. Pickering and T. F. Whale. 2015. Stacking Disorder in Ice I. Phys. Chem. Chem. Phys. 17: 60–76.

Martelli, F., N. Giovambattista, S. Torquato and R. Car. 2018. Searching for crystal-ice domains in amorphous ices. Phys. Rev. Mat. 2: 075601.

Matsui, T., M. Hirata, T. Yagasaki, M. Matsumoto and H. Tanaka. 2017. Communication: Hypothetical ultralow-density ice polymorphs. J. Chem. Phys. 147: 091101.

Matsuo, T. and H. Suga. 1987. Calorimetric study of ices I*h* doped with alkali hydroxides and other impurities. Journal de Physique C1: 477–483.

Mayer, E. and A. Hallbrucker. 1987. Cubic ice from liquid water. Nature 325: 601–602.

McFarlan, R. L. 1936. The structure of ice III. J. Chem. Phys. 4: 253–259.

Militzer, B. and H. F. Wilson. 2010. New phases of water ice predicted at megabar pressures. Phys. Rev. Lett. 105: 195701.

Millot, M., S. Hamel, J. R. Rygg, P. M. Celliers, G. W. Collins, F. Coppari et al. 2018. Experimental evidence for superionic water ice using shock compression. Nat. Phys. 14: 297–302.

Millot, M., F. Coppari, J. R. Rygg, A. Correa Barrios, S. Hamel, D. C. Swift et al. 2019. Nanosecond X-ray diffraction of shock-compressed superionic water ice. Nature 569: 251–255.

Minceva-Sukarova, B., W. F. Sherman and G. R. Wilkinson. 1984. A high pressure spectroscopic study on the ice III - ice IX, disordered—ordered transition. J. Mol. Struct. 115: 137–140.

Minceva-Sukarova, B., W. F. Sherman and G. R. Wilkinson. 1985. Isolated O-D stretching frequencies in ice II. Spectrochim. Acta 41A: 315–318.

Minceva-Sukarova, B., G. E. Slark and W. F. Sherman. 1986. The raman spectra of ice V and ice VI and evidence of partial proton ordering at low temperature. J. Mol. Struct. 143: 87–90.

Minceva-Sukarova, B., G. Slark and W. F. Sherman. 1988. The raman spectra of the KOH-doped ice polymorphs: V and VI. J. Mol. Struct. 175: 289–293.

Mishima, O., N. Mori and S. Endo. 1979. Thermal expansion anomaly of ice VI related to the order-disorder transtion. J. Chem. Phys. 70: 2037–2038.

Moynihan, C. T., P. B. Macedo, C. J. Montrose, P. K. Gupta, M. A. DeBolt, F. J. Dill et al. 1976. Structural relaxation in vitreous materials. Ann. N. Y. Acad. Sci. 279: 15–35.

Murray, B. J., C. G. Salzmann, A. J. Heymsfield, S. Dobbie, R. R. Neely and C. J. Cox. 2015. Trigonal ice crystals in Earth's atmosphere. Bull. Am. Met. Soc. 96: 1519–1531.

Nakamura, T., M. Matsumoto, T. Yagasaki and H. Tanaka. 2016. Thermodynamic stability of ice II and its hydrogen-disordered counterpart: Role of zero-point energy. J. Phys. Chem. B 120: 1843–1848.

Nanda, K. D. and G. J. O. Beran. 2013. What governs the proton ordering in ice XV? J. Phys. Chem. Lett. 4: 3165–3169.

Nelmes, R. J., J. S. Loveday and W. G. Marshall. 1998. Multisite disordered structure of ice VII to 20 GPa. Phys. Rev. Lett. 81: 2719–2722.

Nishibata, K. 1972. Growth of ice IV and equilibrium curves between liquid water, ice IV, ice V and ice VI. Jpn. J. Appl. Phys. 11: 1701–1708.

Nishibata, K. and E. Whalley. 1974. Thermal effects of the transformation ice III-IX. J. Chem. Phys. 60: 3189–3194.

Noguchi, N. and T. Okuchi. 2016. Self-diffusion of protons in H2O ice VII at high pressures: Anomaly around 10 GPa. J. Chem. Phys. 144: 234503.

O'Keeffe, M. 1998. New ice outdoes related nets in smallest-ring size. Nature 392: 879.

Okada, T., T. Iitaka, T. Yagi and K. Aoki. 2014. Electrical conductivity of ice VII. Sci. Rep. 4: 5778.

Parkkinen, P., S. Riikonen and L. Halonen. 2014. Ice XI: Not that ferroelectric. J. Phys. Chem. C 118: 26264–26275.

Pauling, L. 1935. The structure and entropy of ice and other crystals with some randomness of atomic arrangement. J. Am. Chem. Soc. 57: 2680–2684.

Petrenko, V. F. and R. W. Whitworth. 1999. Physics of Ice. Oxford: Oxford University Press.

Pickard, C. J., M. Martinez-Canales and R. J. Needs. 2013. Decomposition and terapascal phases of water ice. Physical Review Letters 110: 245701.

Pistorius, C. W. F. T., E. Rapoport and J. B. Clark. 1968. Phase diagrams of H2O and D2O at high pressures. J. Chem. Phys. 48: 5509–5514.

Polian, A. and M. Grimsditch. 1984. New high-pressure phase of $H_2O$: Ice X. Phys. Rev. Lett. 15: 1312–1314.

Rabideau, S. W., E. D. Finch, G. P. Arnold and A. L. Bowman. 1968. Neutron diffraction study of ice polymorphs. I. Ice IX. J. Chem. Phys. 49: 25142519.

Raza, Z., D. Alfe, C. G. Salzmann, J. Klimes, A. Michaelides and B. Slater. 2011. Proton ordering in cubic ice and hexagonal ice; a potential new ice phase-XIc. Phys. Chem. Chem. Phys. 13: 19788–19795.

Ripmeester, J. A., C. I. Ratcliffe, D. D. Klug and J. S. Tse. 2006. Molecular perspectives on structure and dynamics in clathrate hydrates. Ann. N.Y. Acad. Sci. 715: 161–176.

Ross, R. G., P. Andersson and G. Bäckström. 1978. Effects of H and D order on the thermal conductivity of ice phases J. Chem. Phys. 68: 3967–3972.

Rosu-Finsen, A. and C. G. Salzmann. 2018. Benchmarking acid and base dopants with respect to enabling the ice V to XIII and ice VI to XV hydrogen-ordering phase transitions. J. Chem. Phys. 148: 244507.

Rosu-Finsen, A. and C. G. Salzmann. 2019. Origin of the low-temperature endotherm of acid-doped ice VI: New hydrogen-ordered phase of ice or deep glassy states? Chem. Sci.: 515–523.

Rosu-Finsen, A., A. Amon, J. Armstrong, F. Fernandez-Alonso and C. G. Salzmann. 2020. Deep-glassy ice VI revealed with a combination of neutron spectroscopy and diffraction. J. Phys. Chem. Lett. 11: 1106–1111.

Röttger, K., A. Endriss, J. Ihringer, S. Doyle and W. F. Kuhs. 1994. Lattice constants and thermal expansion of $H_2O$ and $D_2O$ ice Ih between 10 and 265 K. Acta Cryst. B50: 644–648.

Salzmann, C., I. Kohl, T. Loerting, E. Mayer and A. Hallbrucker. 2002a. The raman spectrum of ice XII and its relation to that of a new "High-Pressure Phase of $H_2O$ Ice". J. Phys. Chem. B 106: 1–6.

Salzmann, C. G., T. Loerting, I. Kohl, E. Mayer and A. Hallbrucker. 2002b. Pure ice IV from high-density amorphous ice. J. Phys. Chem. B 106: 5587–5590.

Salzmann, C. G., I. Kohl, T. Loerting, E. Mayer and A. Hallbrucker. 2003a. The low-temperature dynamics of recovered ice XII as studied by differential scanning calorimetry: a comparision with ice V. Phys. Chem. Chem. Phys. 5: 3507–3517.

Salzmann, C. G., I. Kohl, T. Loerting, E. Mayer and A. Hallbrucker. 2003b. Raman spectroscopic study on hydrogen bonding in recovered ice IV. J. Phys. Chem. B 107: 2802–2807.

Salzmann, C. G., T. Loerting, I. Kohl, E. Mayer and A. Hallbrucker. 2003c. Pure ices IV and XII from high-density amorphous ice. Can. J. Phys. 81: 25–32.

Salzmann, C. G., E. Mayer and A. Hallbrucker. 2004a. Effect of heating rate and pressure on the crystallization kinetics of high-density amorphous ice on isobaric heating between 0.2 and 1.9 GPa. Phys. Chem. Chem. Phys. 6: 5156–5165.

Salzmann, C. G., E. Mayer and A. Hallbrucker. 2004b. Thermal properties of metastable ices IV and XII: comparison, isotope effects and relative stabilities. Phys. Chem. Chem. Phys. 6: 1269–1276.

Salzmann, C. G., A. Hallbrucker, J. L. Finney and E. Mayer. 2006a. Raman spectroscopic study of hydrogen ordered ice XIII and of its reversible phase transition to disordered ice V. Phys. Chem. Chem. Phys. 8: 3088–3093.

Salzmann, C. G., A. Hallbrucker, J. L. Finney and E. Mayer. 2006b. Raman spectroscopic features of hydrogen-ordering in ice XII. Chem. Phys. Lett. 429: 469–473.

Salzmann, C. G., P. G. Radaelli, A. Hallbrucker, E. Mayer and J. L. Finney. 2006c. The preparation and structures of hydrogen ordered phases of ice. Science 311: 1758–1761.

Salzmann, C. G., P. G. Radaelli, A. Hallbrucker, E. Mayer and J. L. Finney. 2007. New hydrogen ordered phases of ice. *In*: Kuhs, W. F. (ed.). Physics and Chemistry of Ice. Cambridge: The Royal Society of Chemistry.

Salzmann, C. G., P. G. Radaelli, J. L. Finney and E. Mayer. 2008. A calorimetric study on the low temperature dynamics of doped ice v and its reversible phase transition to hydrogen ordered ice XIII. Phys. Chem. Chem. Phys. 10: 6313–6324.

Salzmann, C. G., P. G. Radaelli, E. Mayer and J. L. Finney. 2009. Ice XV: A new thermodynamically stable phase of ice. Phys. Rev. Lett. 103: 105701.

Salzmann, C. G., P. G. Radaelli, B. Slater and J. L. Finney. 2011. The polymorphism of ice: five unresolved questions. Phys. Chem. Chem. Phys. 13: 18468–18480.

Salzmann, C. G., B. J. Murray and J. J. Shephard. 2015. Extent of stacking disorder in diamond. Diam. Relat. Mater. 59: 69–72.

Salzmann, C. G., B. Slater, P. G. Radaelli, J. L. Finney, J. J. Shephard, M. Rosillo-Lopez et al. 2016. Detailed crystallographic analysis of the ice VI to Ice XV hydrogen ordering phase transition. J. Chem. Phys. 145: 204501.

Salzmann, C. G. 2019. Advances in the experimental exploration of water's phase diagram. J. Chem. Phys. 150: 060901.

Salzmann, C. G., Z. Sharif, C. L. Bull, S. T. Bramwell, A. Rosu-Finsen and N. P. Funnell. 2019. Ammonium Fluoride as a hydrogen-disordering agent for ice. J. Phys. Chem. C 123: 16486–16492.

Shephard, J. J. and C. G. Salzmann. 2015. The complex kinetics of the ice VI to Ice XV hydrogen ordering phase transition. Chem. Phys. Lett. 637: 63–66.

Shephard, J. J., S. Klotz and C. G. Salzmann. 2016. A new structural relaxation pathway of low-density amorphous ice. J. Chem. Phys. 144: 204502.

Shephard, J. J. and C. G. Salzmann. 2016. Molecular reorientation dynamics govern the glass transitions of the amorphous ices. J. Phys. Chem. Lett. 7: 2281–2285.

Shephard, J. J., S. Ling, G. C. Sosso, A. Michaelides, B. Slater and C. G. Salzmann. 2017. Is high-density amorphous ice simply a "Derailed" state along the ice I to Ice IV pathway? J. Phys. Chem. Lett. 8: 1645–1650.

Shephard, J. J., B. Slater, P. Harvey, M. Hart, C. L. Bull, S. T. Bramwell et al. 2018. Doping-induced disappearance of ice II from water's phase diagram. Nat. Phys. 14: 569–572.

Stillinger, F. H. and K. S. Schweitzer. 1983. Ice under pressure: Transition to symmetrical hydrogen bonds. J. Phys. Chem. 87: 4281–4288.

Strobel, T. A., M. Somayazulu, S. V. Sinogeikin, P. Dera and R. J. Hemley. 2016. Hydrogen-stuffed, quartz-like water ice. J. Am. Chem. Soc. 138: 13786–13789.

Sun, J., B. K. Clark, S. Torquato and R. Car. 2015. The phase diagram of high-pressure superionic ice. Nat. Comm. 6: 8156.
Tajima, Y., T. Matsuo and H. Suga. 1982. Phase transition in KOH-doped hexagonal ice. Nature 299: 810–812.
Tajima, Y., T. Matsuo and H. Suga. 1984. Calorimetric study of phase transition in hexagonal ice doped with alkali hydroxides. J. Phys. Chem. Solids 45: 1135–1144.
Takii, Y., K. Koga and H. Tanaka. 2008. A plastic phase of water from computer simulation. J. Chem. Phys. 128: 204501.
Tammann, G. 1900. Über die Grenzen des festen Zustandes. Ann. Phys. 2: 1–31.
Tammann, G. 1910. Über das Verhalten des Wassers bei hohen Drucken und tiefern Temperaturen. ZS. Phys. Chem. 72: 609–631.
Teixeira, J. 1998. The double identity of ice X. Nature 392: 232–233.
Thoeny, A. V., T. M. Gasser and T. Loerting. 2019. Distinguishing ice β-XV from deep glassy ice VI: raman spectroscopy. Phys. Chem. Chem. Phys. 21: 15452–15462.
Tielens, A. G. G. M. 2013. The molecular universe. Rev. Mod. Phys. 85: 1021–1081.
Tran, H., A. V. Cunha, J. J. Shephard, A. Shalit, P. Hamm, T. L. C. Jansen et al. 2017. 2D IR spectroscopy of high-pressure phases of ice. J. Chem. Phys. 147: 144501.
Tribello, G. A., B. Slater and C. G. Salzmann. 2006. A blind structure prediction of ice XIV. J. Am. Chem. Soc. 128: 12594–12595.
Tschauner, O., S. Huang, E. Greenberg, V. B. Prakapenka, C. Ma, G. R. Rossman et al. 2018. Ice-VII inclusions in diamonds: Evidence for aqueous fluid in Earth's deep mantle. Science 359: 1136–1139.
Ueda, M., T. Matsuo and H. Suga. 1982. Calorimetric study of proton ordering in hexagonal ice catalysed by hydrogen fluoride. J. Phys. Chem. Solids 12: 1165–1172.
Vonnegut, K. 1963. Cat's Cradle. New York, USA: Holt, Rinehart and Winston.
Walter, M. L. 1990. Science and Cultural Crisis: An Intellectual Biography of Percy Williams Bridgman (1882–1961). Stanford: Stanford University Press.
Whale, T. F., S. J. Clark, J. L. Finney and C. G. Salzmann. 2013. DFT-assisted interpretation of the raman spectra of hydrogen-ordered ice XV. J. Raman Spectrosc 44: 290–298.
Whalley, E. and D. W. Davidson. 1965. Entropy changes at the phase transitions in ice. J. Chem. Phys. 43: 2148–2149.
Whalley, E., D. W. Davidson and J. B. R. Heath. 1966. Dielectric properties of ice VII. Ice VIII: A New Phase of Ice. J. Chem. Phys. 45: 3976–3982.
Whalley, E., J. B. R. Heath and D. W. Davidson. 1968. Ice IX: An antiferroelectric phase related to ice III. J. Chem. Phys. 48: 2362–2370.
Whalley, E. 1983. Cubic ice in nature. J. Phys. Chem. 87: 4174–4179.
Wilson, G. J., R. K. Chan, D. W. Davidson and E. Whalley. 1965. Dielectric properties of ices II, III, V, and VI. J. Chem. Phys. 43: 2384–2391.
Wollan, E. O., W. L. Davidson and C. G. Shull. 1949. Neutron diffraction study of the structure of ice. Phys. Rev. 75: 1348–1352.
Yoshimura, Y., S. T. Stewart, H.-k. Mao and R. J. Hemley. 2007. *In situ* Raman spectroscopy of low-temperature/high-pressure transformations of H2O. J. Chem. Phys. 126: 174505.
Yu, X., J. Zhu, S. Du, H. Xu, S. C. Vogel, J. Han et al. 2014. Crystal structure and encapsulation dynamics of ice II-structured neon hydrate. Proc. Natl. Acad. Sci. USA 111: 10456–10461.
Zeng, Q., T. Yan, K. Wang, Y. Gong, Y. Zhou, Y. Huang et al. 2016. Compression icing of room-temperature NaX solutions (X = F, Cl, Br, I). Phys. Chem. Chem. Phys. 18: 14046–14054.
Zeng, Q., C. Yao, K. Wang, C. Q. Sun and B. Zou. 2017. Room-temperature NaI/H2O compression icing: solute–solute interactions. Phys. Chem. Chem. Phys. 19: 26645–26650.
Zha, C.-S., J. S. Tse and W. A. Bassett. 2016. New Raman measurements for $H_2O$ ice VII in the range of 300 cm−1 to 4000 cm−1 at pressures up to 120 GPa. J. Chem. Phys. 145: 124315.
Zhao, J., S. L. Simon and G. B. McKenna. 2013. Using 20-million-Year-old Amber to Test the Super-Arrhenius Behaviour of Glass-forming Systems. Nat. Comm. 4: 1783.